Journal of Solid State Chemistry 184 (2011) 1768–1776

Contents lists available at ScienceDirect

Journal of Solid State Chemistry

journal homepage: www.elsevier.com/locate/jssc

Microstructural features and domain formation in $(Ba,Sr)_2TiSi_2O_8$ fresnoites

Chui Ling Wong [a,*], Cristiano Ferraris [b], T.J. White [a,c]

[a] School of Materials Science & Engineering, Nanyang Technological University, Singapore 639798, Singapore
[b] Laboratoire de Mineralogie et Cosmchimie du Muséum National d'Historie Naturelle, UMR-CNRS 7202, CP 52, 61 Rue Buffon, 75005 Paris, France
[c] Centre for Advanced Microscopy, The Australian National University, Canberra ACT 0200, Australia

ARTICLE INFO

Article history:
Received 27 October 2010
Received in revised form
2 May 2011
Accepted 3 May 2011
Available online 8 May 2011

Keywords:
(Ba,Sr)-fresnoite
Incommensuration
TEM
Electron diffraction

ABSTRACT

The formation and co-existence of crystallographically modulated and non-modulated regions in $(Ba,Sr)_2TiSi_2O_8$ fresnoites is reviewed, particularly the dependence on local composition. It is shown that perturbations of the average fresnoite structure, determined from appreciable single crystals, are in some cases better described as nanometric domain intergrowths where departures from ideal stoichiometry are characteristics of incommensuration, while modulation is absent from volumes that are less perturbed chemically. Evidence for this differentiation is obtained from selected area electron diffraction (SAED) patterns and high-resolution transmission electron microscopy (HRTEM) images. The domains are readily distinguished by their unique contrast in bright field electron micrographs. Fourier reconstructions of HRTEM images collected from areas with darker contrast show that modulation can change within relatively small volumes. Nearby areas with lighter contrast were found by SAED to be free of structural disorder and incommensurate reflections.

1. Introduction

An atypical barium titanosilicate mineral from the Eastern Fresno County of California was noted in 1962 [1], and subsequently confirmed by Alfors et al. [2] using powder X-ray diffraction. The type specimen was named fresnoite, and although physical, optical and chemical analyses were performed, the crystallography was unsolved until Moore and Louisnathan [3,4] established that $Ba_2TiSi_2O_8$ (BTS) fresnoite was a layered structure where planes of barium atoms were separated by corner-connected sheets of SiO_4 and TiO_5 polyhedra (Fig. 1). This unusual motif, especially with respect to titanium in square-pyramidal coordination, spurred interest in its magnetic [5–7] and optical properties [8,9].

The development of crystallochemical models for fresnoite has relied heavily on electron diffraction to unequivocally define the super-space groups and modulation vectors. However, several studies have revealed that incommensuration can vary between crystals of the same composition, even when preparative methods are notionally identical. Höche et al. [10] using a combination of single crystal X-ray and electron diffraction reported a range of satellite reflection patterns, even within the same single 'crystal', that unequivocally indicates domain formation.

BTS was not immediately suspected of being incommensurate, even though unusual atomic displacement parameters were extracted by X-ray diffraction [4,11]. However, selected area electron diffraction (SAED) conducted at room temperature readily revealed modulated satellite reflections along ⟨100⟩ at $h\ k\ l\ ½$ levels and a doubling of the parent *c*-axis [12]; incommensurate modulations were found along the a* and the b* directions. Specifically, a transition between commensurate and modulated BTS was reported at 160 °C,

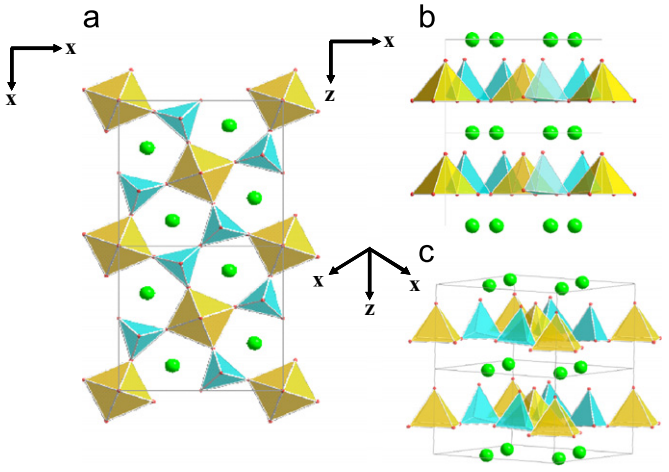

Fig. 1. Fresnoite crystal structure projections. (a) View along [001] emphasizes the corner connected Ti-square pyramids (yellow) and Si-tetrahedra (light blue) (110) slabs. Basal and apical oxygens (red dots) (b) and (c) are separated by 10-fold coordination to alkaline-earth cations (green spheres). (For interpretation of the references to color in this figure legend, the reader is referred to the web version of this article.)

* Corresponding author.
E-mail address: wong0233@e.ntu.edu.sg (C.L. Wong).

0022-4596/$ - see front matter © 2011 Elsevier Inc. All rights reserved.
doi:10.1016/j.jssc.2011.05.009

with the suggestion that the phase boundary migrates through distortion (buckling and tilting) of the corner connected polyhedral network [13], rather than compositional variation.

Table 1
Synthesis of fresnoite-type compounds.

Compound	Sintering temperature (°C)	Sintering period (h)
$Ba_2TiSi_2O_8$	1200	3×12
$Sr_2TiSi_2O_8$	1200	2×12
$(BaSr)_2TiSi_2O_8$	1200	3×12

Electron microscopy confirmed that $Sr_2TiSi_2O_8$ (STS) is also modulated [10,14] and while metrically similar to BTS, STS has two families of satellite reflections at $0.4a^*$, $0.4b^*$, $0.6a^*$ and $0.6b^*$ and additionally at $0.43a^*$, $0.43b^*$, $0.57a^*$ and $0.57b^*$. The origin of the latter satellites suggests that correlations between the polyhedral layers become stronger because strontium is smaller than barium [14]. Single crystal X-ray analysis of STS found a superspace group $P4bm(-\alpha, \alpha, ½; \alpha, \alpha, ½)$ where $\alpha = 0.3$ with $a = 8.312$ Å and $c = 10.07$ Å [10], and a doubling of the layer stacking repeat.

Withers et al. [13] have demonstrated that satellite reflections in fresnoite type structures can arise from prescribed Rigid Unit Mode (RUM) movements of the corner connected polyhedra.

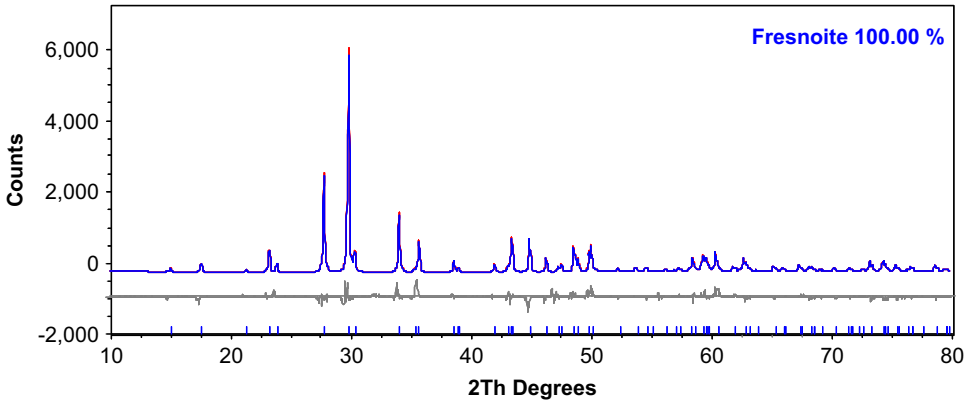

Fig. 2. X-ray diffraction pattern of Sr-fresnoite (STS) powder obtained after multiple firing cycles. Rietveld analysis suggests a high degree of homogeneity.

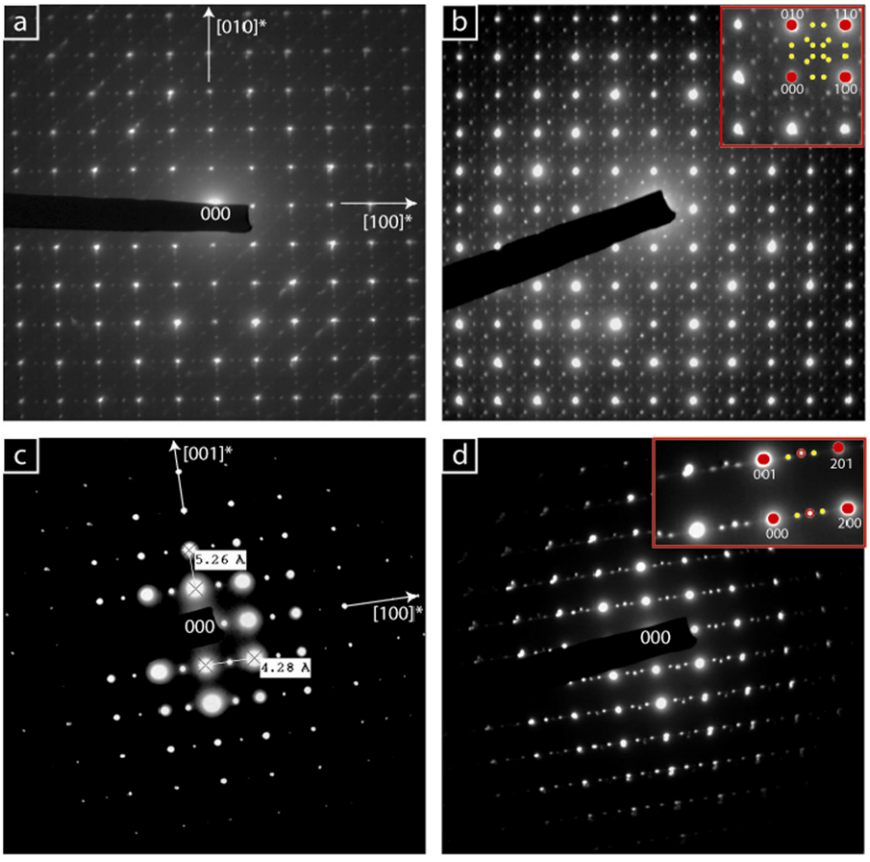

Fig. 3. Selected area electron diffraction patterns of Sr-fresnoite (STS) along both [001] and [010] from volumes with almost homogeneous bright contrast (a) and (c), and from portions showing dark contrast (b) and (d), respectively. For volumes where high intensities of incommensurate reflections are observed figure insets are presented (b, d). For both insets, red disks and open red circles correspond to kinematical and dynamical family reflections common to all fresnoite family members, respectively; smaller yellow disks represent incommensurate reflections showing the same geometrical distribution already described by Höche et al. [10]. (For interpretation of the references to color in this figure legend, the reader is referred to the web version of this article.)

This analysis assumes the polyhedra are difficult to deform, and it is energetically preferable to rotate these units about [001] to relieve stress within the sheets. In this manner, rigid body displacements lead to phase transitions and polymorphism.

Most observations concerning synthetic incommensurate fresnoite and natural analogs are from single crystals produced from melts [12–14] or large mineral species [15]. It was assumed that melting produces chemically homogeneous and thermodynamically stable materials [13], and that commensurate–incommensurate phase transitions could be promoted by adjusting annealing time and temperature [16]; indeed, given the subtle changes in the oxygen sub-lattice involved, different degrees of order-disorder might be expected simultaneously at nanometer and micrometer scales of nominally single crystals. Further investigation revealed the correlation of phase transformations on ionic ordering [17], while another study found geometrical charge frustration could lead to modulation [18]. Alternatively, a collective nucleation mechanism has been proposed to explain the co-existence of commensurate and

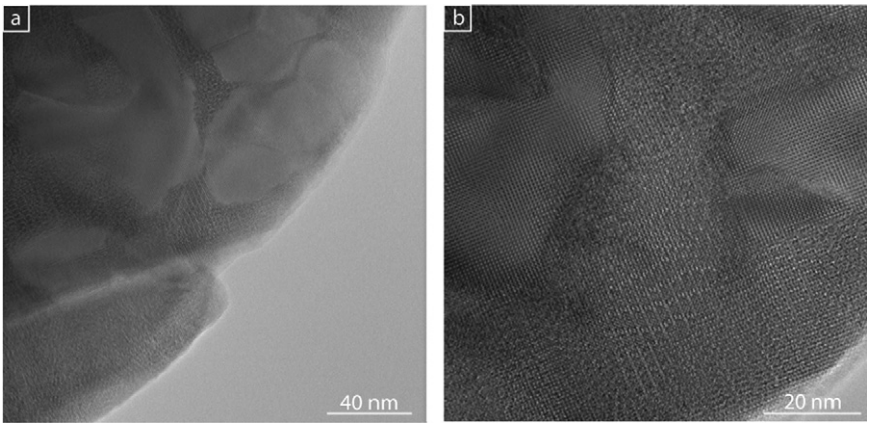

Fig. 4. (a) [001] TEM images of the Sr-fresnoite powder sample where irregularly shaped dark contrast areas are bounded by wider areas where the contrast is more homogeneous and brighter. (b) [001] HRTEM image clearly showing the higher degree of structural disorder characterizing the dark contrast volumes compared to areas where the Sr-fresnoite structure is ordered (bright parts).

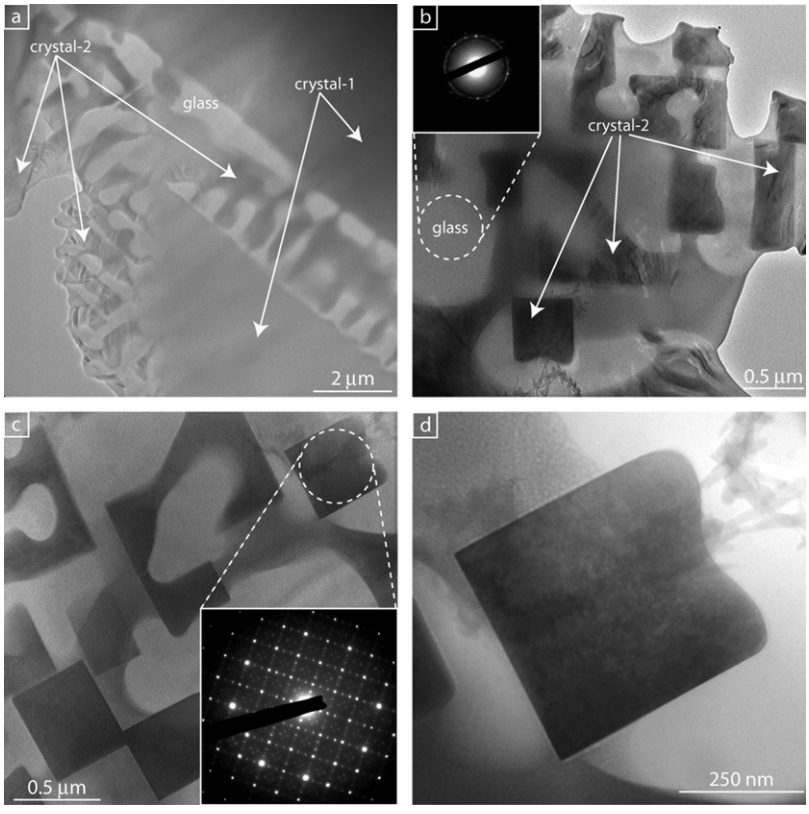

Fig. 5. Low magnification TEM images of an ion milled sample. (a) Skeletal crystals (crystal-2) growth within a glassy ground mass separating volumes with the same bright uniform contrast (crystal-1). (b) Idiomorphic darker contrast crystalline material (crystal-2) is present within a lighter contrast non-crystalline ground mass as revealed by SAED (inset). (c) Electron diffraction reveals that both skeletal and idiomorphic crystals within the glassy ground mass are characterized by the constant presence of incommensurate reflections testifying that almost the entire structure is characterized by a high degree of disorder. (d) The high degree of structural disorder is evident for higher magnification images where a very fine and patchy distribution of contrast appears within both skeletal and small idiomorphic crystals.

incommensurate phases, suggesting a continuous transition [19]. The appearance of domains impacts upon the reliability of Rietveld refinements commonly used in materials science studies, and specifically impede the investigation of anisotropic thermal parameters and possible cation ordering.

The majority of fresnoite investigation is concerned with appreciable single crystals or glass ceramic thin films, where crystallochemical characterization of these complex oxides is somewhat simpler. However fresnoite photocatalyts and solid electrolytes are beginning to receive attention. These materials are either fine powders or polycrystalline ceramics, and these physical forms are not so readily evaluated, especially with respect to incommensuration, although these fundamental properties will direct functional properties. To address this, we here present a microstructural, electron diffraction and high resolution electron microscopy study of Ba-fresnoite (BTS) and Sr-fresnoite (STS), and a mixture of Ba,Sr-fresnoite (BSTS) is presented. It is confirmed that incommensurate modulations are stoichiometrically dependent and moreover, it is suggested that STS, previously described as a homogeneous single crystal, may be better visualized as nanometric intergrowths of commensurate and incommensurate domains.

2. Experimental methods

2.1. Sample preparation

The starting materials for solid state synthesis were oxides (anatase-TiO_2-Aldrichm, AR grade), carbonates ($BaCO_3$-Fisher, 99.6%, $SrCO_3$-BDH, 98.5%) and silicic acid (H_2SiO_3-Sino, 99%). These were manually mixed in stoichiometric proportions using an agate mortar and pestle, before preparing pellets and sintering in air (Table 1). Powder X-ray diffraction (XRD) showed that intermediate phases were removed by repeated cycles of grinding, pelletizing and sintering to obtain (nearly) single phase products (Fig. 2) through incipient melting and wetting that accelerated mass transport.

After final annealing, two sample sets were prepared for transmission electron microscopy (TEM): a collection of powdered materials deposited on holey-carbon coated copper-grids, and a suite of argon ion milled portions of sintered pellets. For milling, 3 mm Ø disks were trepanned using an ultrasonic cutter. These were finely polished with diamond paste before gluing onto a copper washer using epoxy, mechanically dimpled and finally perforated high precision ion milling. To minimize charging during electron microscopy, the samples were coated with a thin film of evaporated carbon.

2.2. Electron microscopy

TEM was conducted at 200 kV using a JEOL JEM-2100F TEM (C_s=0.5 mm). High-resolution images were collected using an objective aperture of 20 μm, corresponding to a nominal point-to-point resolution of 0.17 nm. In order to verify the stoichiometry, all crystals were analyzed semi-quantitatively in the TEM-energy dispersive spectroscopy (TEM-EDS) mode, with a live counting time of 100 s and a nominal beam diameter <5 nm. Recalculation and normalization of the analytical electron microscopy (AEM) analyses were performed assuming the thin-film approximation calibrated against oxide standards. Image processing and simulations for TEM images were carried out using CRISP [20] and JEMS [21], respectively. X-ray maps were collected from the ion milled samples using a low vacuum scanning electron microscope (JEOL JSM 5410LV) operating at 20 keV, while backscattered electron (BSE) images were collected using a scanning electron microscope (SEM) (JEOL JSM 5310) working at 15 keV.

3. Electron crystallography and microstructure

3.1. Sr-fresnoite (STS)

3.1.1. Powdered sample

Selected area electron diffraction (SAED) patterns collected in [001] and [010] zones contain the features observed by Höche et al. [10], but under identical instrumental parameters (i.e. SAED aperture, spot size, sample thickness and illumination conditions), the intensity of the satellite reflections varied regionally from very weak (Fig. 3a and c) to intense (Fig. 3b and d), while the sub-cell (parent) reflections showed no such effects (beyond those expected from curvature of the Ewald sphere).

When high resolution (HR) electron imaging was used, it became clear that incommensurate reflections were stronger for crystal areas containing dark contrast (Fig. 4a), while the satellites were nearly absent in areas with homogeneous bright contrast. Overall, darker areas were much less abundant compared to bright regions; image analyses from several crystals found about 10–15% of the former vs. 90–85% of the latter. Fig. 4b shows a crystal where differences in contrast delineate volumes with considerable structural disorder (dark contrast) and portions were the STS is unaffected by defects, stacking faults or twinning (bright contrast). AEM analyses found the defective portions to be depleted in strontium and silicon, and relatively enriched in titanium compared to non-modulated bright contrast areas. The Sr- and Si-deficits are in the range of 0.6–0.8 and 0.2–0.4 apfu, respectively, while titanium shows an excess of about 0.3–0.5 apfu, with respect to the nominal $Sr_2TiSi_2O_8$ composition.

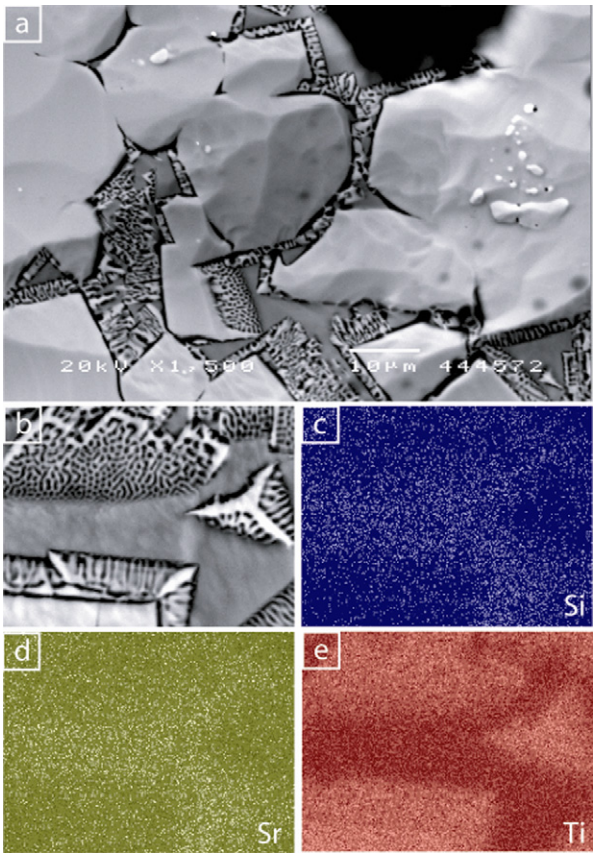

Fig. 6. SEM images and EDX elemental maps of ion milled samples. Both secondary (a) and BSE images (b) clearly show the presence of intra-crystalline domains (light gray) where a quenched structure characterized by the presence of skeletal crystals plunged with a glassy matrix (mesostasis) is visible. X-ray EDS mapping of intra-crystalline areas reveal that the glassy matrix is slightly enriched in both Si (c) and Sr (d) while clearly depleted in Ti (e).

Together with these dominant contrast distributions were a few percent (~1–3%) of homogeneous and very bright contrast areas, that SAED showed were poorly crystalline as indicated by diffuse diffraction rings and the absence of Bragg spots. The ring positions were variable and could not be indexed to published crystallographic data for oxides of Sr, Si and Ti in any combination.

3.1.2. Ion-milled sample

TEM images of the ion milled fresnoites contain intriguing structures where areas of bright uniform contrast (hereafter named crystal-1), were separated by a herringbone structure (Fig. 5a). More rarely idiomorphic crystalline material with darker contrast (crystal-2) is embedded in the non-crystalline ground mass revealed by SAED (Fig. 5b). AEM analyses indicate that all three crystal morphologies correspond to Sr-fresnoite, while the amorphous regions are extremely poor in Ti and therefore enriched in Sr and Si. Chemical analyses of crystal-2, as were already observed for dark contrast areas of the powder samples, are deficient in Sr and Si contents and Ti-enriched.

SAED of crystal-1 show the characteristics of the powder samples, with the skeletal and/or idiomorphic crystals invariably yielding strong satellite reflections (Fig. 5c). In general, TEM images of crystal-2 have uniform contrast (Fig. 5c), but enhancing diffraction contrast clearly provides evidence of mottled bright and dark areas (Fig. 5d) that were too small to be examined by SAED and proved exceedingly beam sensitive when attempting convergent beam electron diffraction (CBED). Another common observation for the idiomorphic crystal-2 is that, curved and irregular contrast bands run through the thinnest regions and change in both intensity and position as the diffraction conditions are altered (Fig. 5b).

SEM-EDS analysis of the ion milled material shows that the structures observed by TEM are part of a larger scale growth phenomenon (Fig. 6a), where most of the volumes between the micrometric-sized Sr-fresnoite grains contain amorphous regions in which STS skeletal crystals are embedded. BSE images (Fig. 6b) together with EDS analyses and X-ray elemental mapping (Fig. 6c–e) are consistent with AEM. In particular, X-ray elemental mapping confirmed that the non-crystalline volumes are significantly depleted in titanium and slightly enriched in strontium and silicon. Recently, Wisiewski et al. [27] reported similar structures in fresnoite-bearing glass ceramics containing excess silica and having the overall composition $Ba_2TiSi_{2.75}O_{9.5}$.

3.2. Powdered Ba-fresnoite (BTS)

Because STS powders and ion-milled sections revealed unexpected spatial and chemical features of incommensurability, BTS was examined to establish if these phenomena were generic. The satellite reflections of BTS are similar to those of STS during SAED [13] but less intense than in single crystal X-ray diffraction (Fig. 7) [10]. The strength of the satellites could be enhanced by the standard method of tilting slightly off the [001] axis (Fig. 7B).

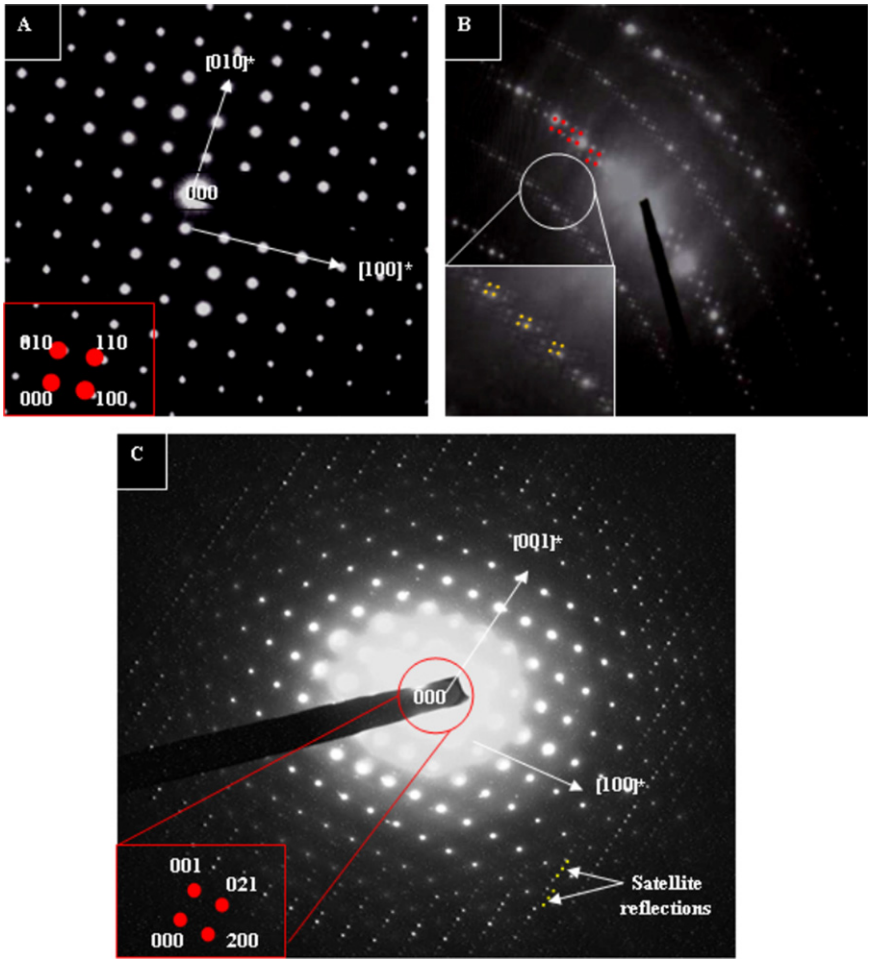

Fig. 7. Electron diffraction of Ba-fresnoite along [001] and [010] from areas with almost homogeneous bright contrast (A) and (B), and from portions showing dark contrast (C). The intensities of incommensurate reflections along [001] are not pronounced. Tilting off-axis is necessary to enhance the weaker reflections. By capturing a larger set of diffraction spots, satellite reflections are observed in the [100] direction. The red disks (inset) correspond to kinematical reflections common to all fresnoite family members, while smaller yellow disks represent incommensurate reflections. (For interpretation of the references to color in this figure legend, the reader is referred to the web version of this article.)

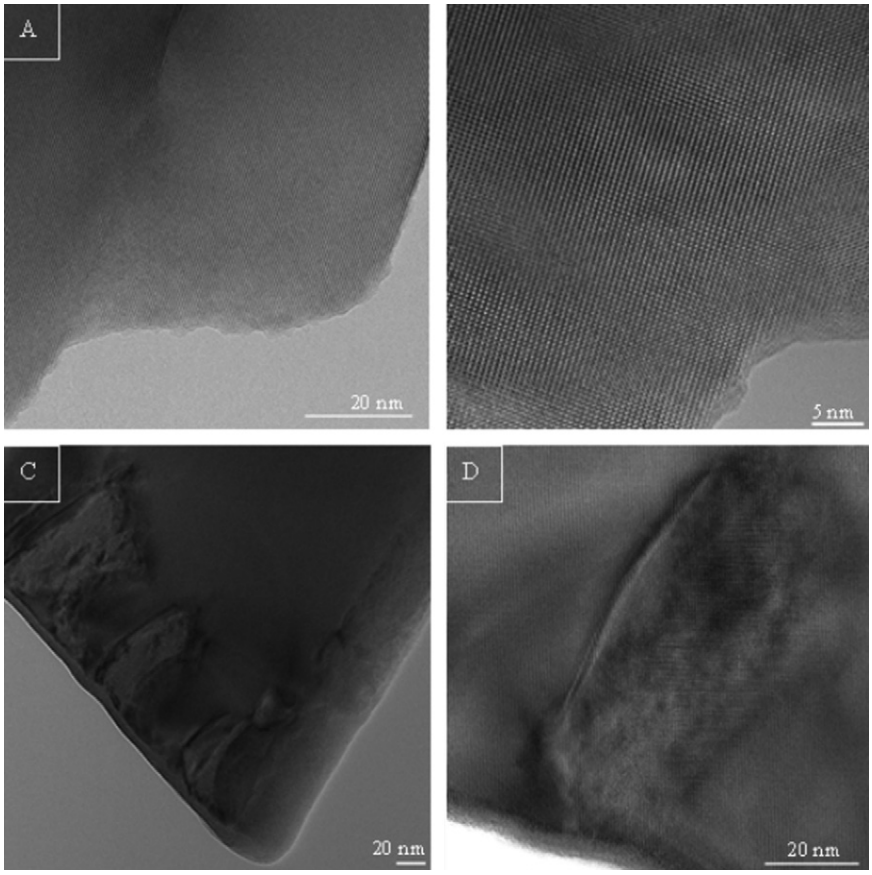

Fig. 8. High resolution imaging of Ba-fresnoite powder along [001] (A) and (B), and [100] (C) and (D). Modulation along [001] perhaps are too weak to be reconstructed while strong modulation is observed along [100] with regions of commensurate (lighter contrast) and incommensurate (darker contrast) phases. (B) and (D) are the enlargements of (A) and (C), respectively.

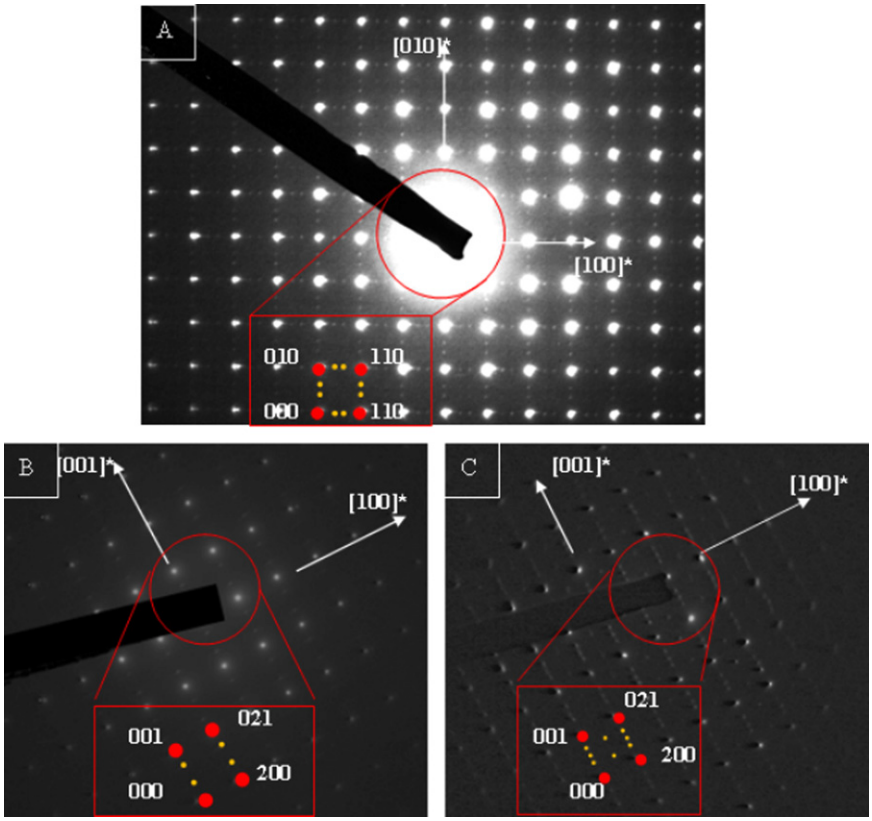

Fig. 9. Electron diffraction of BaSr-fresnoite along both [001] and [010]. Intensities for incommensurate reflections along [001] are not pronounced as in STS. [100] diffraction patterns (B and C) show two sets of diffractions spots after prolonged observation. The red disks (inset) correspond to kinematical sub-cell reflections; smaller yellow disks represent incommensurate reflections. (For interpretation of the references to color in this figure legend, the reader is referred to the web version of this article.)

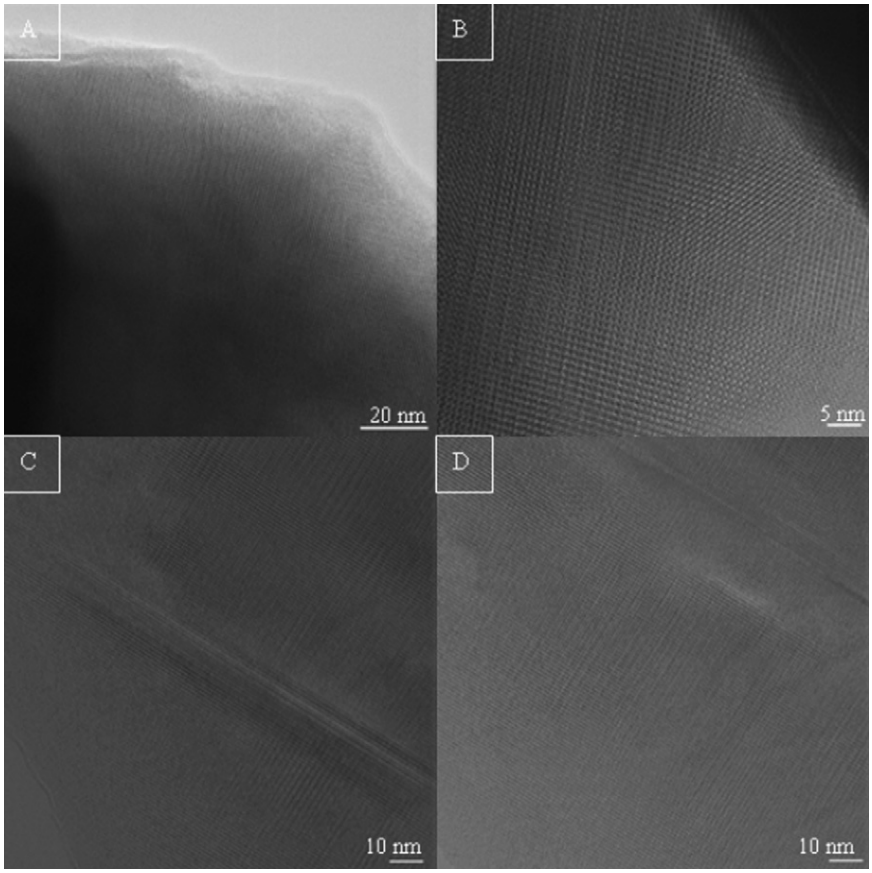

Fig. 10. High resolution imaging of BSTS powder along [001] (A) and (B), and [100] (C) and (D). Modulation along [001] shows the co-existence of commensurate (lighter contrast) and incommensurate (darker contrasts) regions. The [100] incommensurate regions along [100] change during electron irradiation. Micrograph (B) is the enlargement of (A), while (C) and (D) show the change in modulation after short (C) and long (D) illumination.

Moreover, HRTEM imaging of BTS exhibits the same variable regional contrast as STS due to intergrowth of commensurate and incommensurate domains (Fig. 8C and D). These features are readily observed in [100] but are not so apparent in [001] (Fig. 8A and B).

3.3. Powdered Ba,Sr-fresnoite (BSTS)

The electron diffraction patterns of BSTS suggest a more complex modulation than the fresnoite end-members; although [001] was similar, the [100] zones are distinct. The material was noticeably electron beam sensitive and SAED intensity changed after a few minutes observation. Further work is needed to determine if displacive (mainly oxygen) and occupational (barium–strontium) modulations are occurring concurrently. Similar to the fresnoite end-members, BSTS patterns can be indexed as a combination of commensurate and incommensurate reflections. However, as shown in Fig. 9, extracting reliable information from HRTEM without artifacts is problematic, and it is evident that the strength and distribution of satellite spots changed after prolonged observation (Fig. 10).

4. Discussion

4.1. The role of Sr/Si and Ti occupancy in modulation

HRTEM of powdered and ion milled STS found modulated and non-modulated domains at nano- to micro-metric scales (Fig. 4). Fourier reconstruction from different regions shows the satellite reflections and distributions are variable (Fig. 11), and because this heterogeneity extends to a fine scale, the reconstruction of the real structure is challenging. It is evident that incommensuration and contrast arising from stress are correlated (Fig. 4b), and the intensity and position of the bands vary as the diffraction conditions change (i.e. sample tilting). It is presumed strain arises to relieve mismatch induced by the co-existing 3D and higher dimensional volumes; the modulated parts are strontium-poor, which induces local changes in cation–anion bond lengths. These re-arrangements will be accompanied by polyhedral tilting and/or rotation [13] as the mechanism for stress propagation. Most probably in tandem, Ti-rich fresnoite will co-exist with the Ti-poor intergranular ground mass accompanied by the substitution of Si by Ti in tetrahedral coordination as reported by Coats et al. [30].

The bright, undifferentiated contrast of commensurate regions suggests stress is minimal, although bound between incommensurate contoured domains (Fig. 5). This phenomenon may be analogous to the incommensurate walls [22] observed in high temperature superconductors that are postulated to arise from misfit dislocations appearing near the stress bands [23]. In STS, similar defects may be necessary to relieve the stress induced by atomic modulation that accompanies Sr depletion. As observations from powdered BTS and BSTS are similar to STS, the role of Sr/Ba, Ti and Si occupancy/displacement in modulation may be inferred to broadly correspond.

4.2. Ionic ordering in modulated phases

It can be concluded that regional differences in satellite reflection intensity for the [100]/[010] zones (Fig. 3) of STS probably originated from the disordered intergrowth of compositionally differentiated incommensurate regions within the parent structure; for the ion

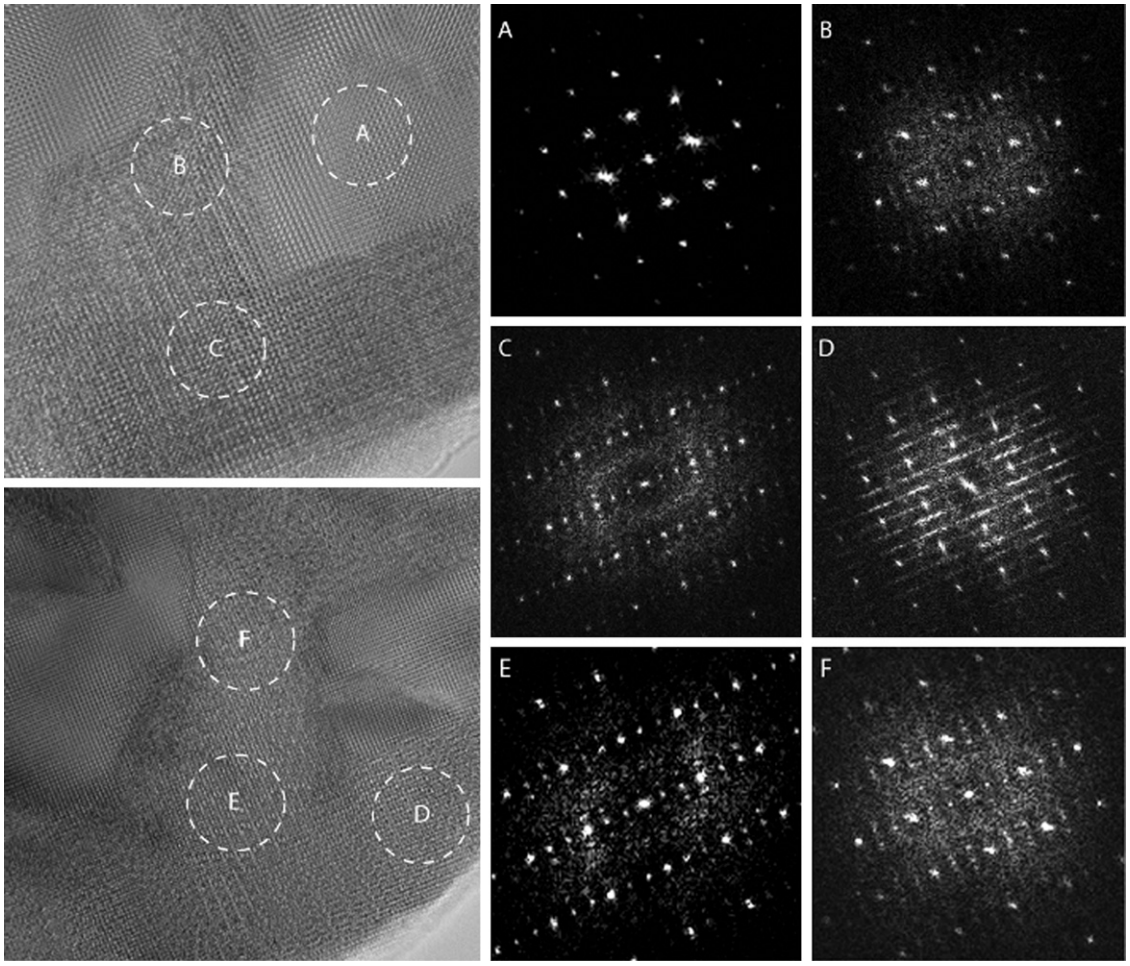

Fig. 11. Two HRTEM images used to reconstruct Fourier Transforms (FT) from different sample areas using the program CRISP. Calculated FT from areas showing different degrees of disorder (i.e. different contrast distributions) clearly demonstrate that incommensuration is heterogeneously distributed. Besides the presence of clearly commensurate areas (A), there are regions showing darker contrast related to different degrees of structural disorder and modulation (B–F).

milled samples (Fig. 5b–f) variations in satellite reflection intensity could be observed in the same "crystal". This suggests different degrees of polyhedral distortion, tilting and/or rotation (RUM mode) [13] induce stresses that create pronounced and/or diffuse boundaries between modulated phases. As significant stoichiometric anomalies are common, more complex phase combinations of the form of $Sr_{2-x}Ti_{1+y}Si_{2-y}O_{8-x}$ cannot be excluded. For example, both $Sr_2Ti_2Si_4O_{14}$ [28] and matsubaraite ($Sr_4Ti_5Si_4O_{22}$) [S.G *C2/m*; $a=13.850$ Å, $b=5.631$ Å, $c=11.892$ Å and $\beta=114.143^\circ$] [24] contains structural elements in common with fresnoite, and incorporation of trans-structural regions may provide a mechanism to relieve strain.

Although materials were prepared via solid state reaction, the skeletal crystal morphology (Fig. 5) within glass suggests incipient melting occurred, as is typical of high temperature systems quenched very rapidly such as glass mesostasis in chondritic meteorites [25,26]. Here, direct quenching of the bulk was not used; however, the multiple grinding and firing steps may have lead to a similar structure. Alternatively, it is well known that fresnoites rapidly crystallize and this may leave a silica-rich melt [29]. In such systems, kinetics rather than thermodynamics controls the reaction products as the temperature drops. In the first stage, when cooling rates are very high, only a few crystal germs attain the critical mass to continuously grow; simultaneously, the crystal structure relaxes to eliminate strain (i.e. removal of ionic disorder or crystal defects). As the temperature diminishes ionic migration rates tend to zero, which captures the skeletal structures within the amorphous titanium poor matrix, and the capability to eliminate structural strain within incommensurate domains. This scenario is in agreement with early observations of BTS where incommensurate domains present at room temperature are removed by heating to $>160\,^\circ$C [13]. The presence of irregularly shaped modulated domains within crystal-1 and, moreover, the strong incommensuration shown by late-formed skeletal crystal-2 show that for STS, and probably BTS and BSTS, the first stage crystallization of incommensurate structures is followed by a partial reorganization that continues until ion mobility slows and freezes the domains. In the last stage, the system retains sufficient energy to nucleate numerous crystallites (the skeletal crystals) but not to sustain crystal growth and structural reorganization that would lead to homogeneous crystal modulation.

Although single crystal melt growth yields improved crystal homogeneity, microscopy suggests that even here domains exist, although these may not be linked to compositional variation. In syntheses conducted near-solidus the phase evolution is more clearly seen from the morphology of the skeletal crystals, which is comparable to mesostasis in meteorites.

5. Conclusion

For the barium and strontium fresnoites studied here, chemical inhomogeneities were characteristics of incommensurate regions, while commensurate regions displayed a stoichiometry less perturbed from $A_2BC_2O_8$. Evidence for this phenomena is directly visible in selected area electron diffraction (SAED) and also captured

via high-resolution transmission electron microscopy (HRTEM) images, but would not be detected by bulk diffraction methods (i.e. X-ray and neutron diffraction) where an "average" structure is recognized; it is unlikely that modeling algorithms can be devised to better extract microstructural content from these latter techniques. Incommensurate and commensurate areas are readily separated by their different degrees of modulation. Fourier reconstructions of HRTEM images captured in the modulated regions showed distinct variations in incommensurability, while SAED patterns from areas without structural disorder do not show satellite reflections. To summarize, in STS a mechanism is proposed to explain the co-existence of both commensurate and non-commensurate phases. HRTEM clearly shows the formation of these domains with AEM analysis supporting stress induced domain formations in Sr depleted regions. These conclusions can be extended to BTS and BSTS that have similar HRTEM images and SAD patterns.

References

[1] O.I. Joensuu, N.H. Suhr, Appl. Spectrosc. 16 (1962) 101–104.
[2] J.T. Alfors, M.C. Stinson, R.A. Matthews, A. Pabst, Am. Mineral. 50 (1965) 314–340.
[3] P.B. Moore, J. Louisnathan, Science 156 (1967) 1361–1362.
[4] P.B. Moore, J. Louisnathan, Z. Kristallogr. 130 (1968) 438–448.
[5] G. Liu, J.E. Greedan, J. Solid State Chem. 114 (1995) 499–505.
[6] R.C. Rai, J. Cao, J.L. Musfeldt, D.J. Singh, X. Wei, R. Jin, Z.X. Zhou, B.C. Sales, D. Mandrus, Phys. Rev. B 73 (2006) 075112.
[7] A. Halliyal, A.S. Bhalla, L.E. Cross, Ferroelectrics 62 (1985) 3–9.
[8] K. Ramesh, J. Gopalakrishnan, Solid State Sci. 3 (2001) 113–119.
[9] Y. Takahashi, K. Kitamura, Y. Benino, T. Fujiwara, T. Komatsu, Appl. Phys. Lett. 86 (2005) 091110.
[10] T. Höche, W. Neumann, S. Esmaeilzadeh, R. Uecker, M. Letzen, C. Rüssel, Solid State Chem. 166 (2002) 15–23.
[11] R. Masse, J.C. Grenier, A. Durif, Bull. Soc. Fr. Miner. 90 (1967) 20–23.
[12] S.A. Markgraf, C.A. Randall, A.S. Bhalla, R.J. Reeder, Solid State Commun. 75 (1990) 821–824.
[13] R.L. Withers, Y. Tabira, Y. Liu, T. Höche, Phys. Chem, Minerals 29 (2002) 624–632.
[14] T. Höche, C. Rüssel, W. Neumann, Solid State Commun. 110 (1999) 651–656.
[15] L. Bindi, M. Dusek, V. Petricek, P. Bonazzi, Acta Cryst. B62 (2006) 1031–1037.
[16] M. Valant, B. Jančar, U. Pirnat, D. Suvorov, J. Eur. Ceram. Soc. 25 (2005) 2829–2834.
[17] U. Pirnat, M. Valant, B. Jančar, D. Suvorov, Chem. Mater. 17 (2005) 5155–5160.
[18] M. Angst, R.P. Hermann, W. Schweika, J.-W. Kim, P. Khalifah, H.J. Xiang, M.H. Whangbo, D.H. Kim, B.C. Sales, D. Mandrus, Phys. Rev. Lett. 99 (2007) 256402.
[19] K. Parlinski, Sci. Rep. RITU A43 (1997) 51–53.
[20] H. Swen, Ultramicroscopy 41 (1992) 121–135.
[21] P. Stadelmann, JEMS, 12M-EPFL, CH-1015 Lausanne, Switzerland, 2003.
[22] J.W. Lee, D.E. Laughlin, Phys. Rev. B 41 (1990) 4093–4097.
[23] J.A. Venables, P.S. Schabes-Retchkiman, Surf. Sci. 71 (1978) 27–41.
[24] H. Miyajima, R. Miyawaki, K. Ito, Eur J. Mineral 14 (2002) 1119–1128.
[25] R.T. Dodd, Meteorites: A Petrologic–Chemical Synthesis, Cambridge University Press, Cambridge, UK, 1981.
[26] C. Ferraris, L. Folco, M. Mellini, Meteorit. Planet. Sci 37 (2002) 1299–1322.
[27] W. Wisniewski, M. Nagel, G. Volksch, C. Russel, Cryst. Growth Design (2010) 4526–4530.
[28] T. Berger, K-J. Range, Z. Naturforsch B51 (1996) 1099–1103.
[29] A.A. Cabral, V.M. Fokin, E.D. Zanotto, Cr. Chinaglia, J. Non-Crystal. Solids 330 (2003) 174–186.
[30] A.M. Coats, N. Hirose, J. Marr, J. Solid State Chem 126 (1996) 105–107.